

ExBEHRT: Extended Transformer for Electronic Health Records to Predict Disease Subtypes & Progressions

Maurice Rupp

*Novartis Oncology AG
Basel, Switzerland*

MAURICE.RUPP@GMAIL.COM

Oriane Peter

*Novartis Oncology AG
Basel, Switzerland*

ORIANE.PETER@GMAIL.COM

Thirupathi Pattipaka

*Novartis Oncology AG
Basel, Switzerland*

THIRUPATHI.PATTIPAKA@NOVARTIS.COM

Abstract

In this study, we introduce ExBEHRT, an extended version of BEHRT (BERT applied to electronic health records), and apply different algorithms to interpret its results. While BEHRT considers only diagnoses and patient age, we extend the feature space to several multimodal records, namely demographics, clinical characteristics, vital signs, smoking status, diagnoses, procedures, medications, and laboratory tests, by applying a novel method to unify the frequencies and temporal dimensions of the different features. We show that additional features significantly improve model performance for various downstream tasks in different diseases. To ensure robustness, we interpret model predictions using an adaptation of expected gradients, which has not been previously applied to transformers with EHR data and provides more granular interpretations than previous approaches such as feature and token importances. Furthermore, by clustering the model representations of oncology patients, we show that the model has an implicit understanding of the disease and is able to classify patients with the same cancer type into different risk groups. Given the additional features and interpretability, ExBEHRT can help make informed decisions about disease trajectories, diagnoses, and risk factors of various diseases.

1. Introduction

Over the past decade, electronic health records (EHRs) have become extremely popular for documenting a patient’s medical history, with many existing records combining heterogeneous temporal information about diagnoses, procedures, laboratory tests, observations and demographic data from a variety of sources (primary care, hospital visits, etc.). In general, a sequence of medical events of a single patient is referred to as a *patient journey*. Given the immense amount of data available (datasets range up to over 100M patients) and its level of detail, there is incredible potential for the use of machine learning to provide new insights into disease pattern recognition, early detection of rare diseases, and personalised risk prediction and treatment planning.

Embedding algorithms derived from natural language processing (NLP) have shown remarkable performance when trained to represent patients’ medical histories. Due to the

chronological structure of EHRs, such algorithms can provide various insights into disease trajectories and clinical phenotypes. Recent advances in NLP have also shown that transformer-based methods such as BERT (Devlin et al. (2018)), GPT-3 (Brown et al. (2020)) and their variations are significantly superior to other approaches, as they are able to model complex temporal dependencies over a long period of time.

In this paper, we present a novel approach to incorporate multimodal features into Transformer models by adding medical concepts separately and vertically, rather than chaining all concepts horizontally. We show that these features are important in various downstream applications such as mortality prediction, patient subtyping and disease progression prediction.

Generalizable Insights about Machine Learning in the Context of Healthcare

The main contributions from this work can be summarized as follows:

1. A novel form of incorporating any sort of multi-modal EHR features into BERT (or any other Transformer-based model) without having to extend the resources needed to train the model due to consistent, fixed patient journey sequences.
2. The addition of patient information that, to our knowledge, was not included in any previous work (BMI, smoking status, laboratory values) and improves model performance for several downstream tasks. These additional features provide a more comprehensive and complex understanding of patients, leading to deeper and more robust insights for clinicians when interpreting model results. In combination with the expected gradients model explainability, we can gain new insights into the different pieces of information and their impact on the outcome.
3. An exploration of unsupervised clustering of cancer patients using the patient representation of ExBEHRT, identifying groups of cancer types and subgroups within one cancer type with diverse information about their characteristics for recognizing risk subtypes and treatment patterns.

2. Related Work

Recent studies have adapted transformers to structured EHR data and shown their superiority in various benchmarks compared to other similar algorithms (Kalyan et al. (2022)). Since most publications in this area are a derivative of BERT (Devlin et al. (2018)), in this section we will focus exclusively on BERT-based approaches applied to EHR data.

The first adaptation of EHR to BERT, called BEHRT (Li et al. (2020)), incorporated diagnosis codes and ages from EHRs and added additional embeddings to separate individual visits (segment embedding) and a position embedding for the visit number. To separate visits, the authors added **SEP** tokens¹ between visits, analogous to the **SEP** token between sentences in BERT and **CLS** token as an artificial start token. The model was pre-trained by using the Masked Language Modelling (MLM) objective on diagnosis concepts.

Med-BERT (Rasmy et al. (2021)) introduced a code serialisation embedding in addition to

1. In NLP, tokens usually refer to the smallest unit into which an input is decomposed. This can be a word, part of a word or, as in this case, a medical concept

diagnosis and position embeddings, indicating the order of diagnoses within a visit. Med-BERT was pre-trained with MLM and a binary classification target of whether a patient had at least one hospital stay of more than one week (*prolonged length of stay in hospital* or PLOS).

CEHR-BERT (Pang et al. (2021)) and BRLTM (Meng et al. (2021)) contain many more measures than the other two approaches. Instead of separate a diagnosis embedding, the studies combined all medical concepts (i.e. conditions, procedures and medications) of a patient into a single vector. This method results in considerable overhead when training a model, as the maximum length of the patient journey is significantly higher than if only the diagnosis codes were included. Adding more features (e.g. observations) would increase the resources required due to the increased length of the vector.

In addition, there are a variety of models that either combine the BERT architecture with other machine learning models (Shang et al. (2019), Poulain et al. (2022), Li et al. (2021)) or focus exclusively on specific use cases (Azhir et al. (2022), Prakash et al. (2021), Rao et al. (2022)).

All the aforementioned approaches either lack generalizability to different domains due to specific pre-training (a key advantage of transfer learning using transformers), do not incorporate enough variety in patient information to generate informed decisions or are limited in the amount of data of a single patient they can process.

3. ExBEHRT for EHR Representation Learning

ExBEHRT is an extension of BEHRT where medical concepts are not concatenated into one long vector (as in Figure 2 for the example patient shown in Figure 1), but grouped into separate, learnable embeddings per concept type. In this way, we avoid exploding input lengths when adding new medical features and give the model the opportunity to learn which concepts it should focus on. From a clinical perspective, it would also be stringent to separate diagnoses, procedures, drugs, etc., as they have different clinical value for downstream applications. We take the number of diagnoses in a visit as an indicator of how many "horizontal slots" are available for other concepts in that visit (e.g. two for the first visit in Figure 3). Therefore, the maximum length of the patient journey is defined by the number of diagnosis codes of a patient, regardless of the number of other concepts added to the model.

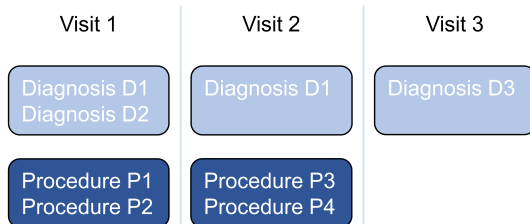


Figure 1: An example of the procedures and diagnoses of a patient with three visits.

As shown by the procedures in figure 3, but carried out in the same way with lab tests, there are three possible cases of adding a new concept to a visit:

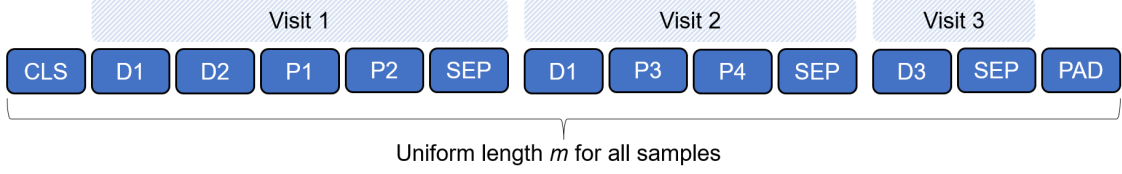


Figure 2: An example of how models like CEHR-BERT and BRLTM represent the patient from figure 1 by horizontally stacking all features into a 1D representation. Note that each additional measure potentially increases the maximal sentence length m .

- a) The number of procedures is equal to the amount of horizontal slots available in the visit (visit 1 - two each). The procedures can therefore be represented as a 1D vector.
- b) The number of procedures exceeds the amount of slots available in the visit (visit 2 - one diagnosis, two procedures). Here, the procedures fill up the number of horizontal slots line by line until there are no more procedures left, resulting in a 2D vector of dimensions $\#slots \times \lceil \frac{\#procedures}{\#slots} \rceil$.
- c) The number of procedures subceeds the amount of slots available (visit 3 - one diagnosis, no procedures). The procedures are represented as a 1D vector and then padded to the amount of horizontal slots available.

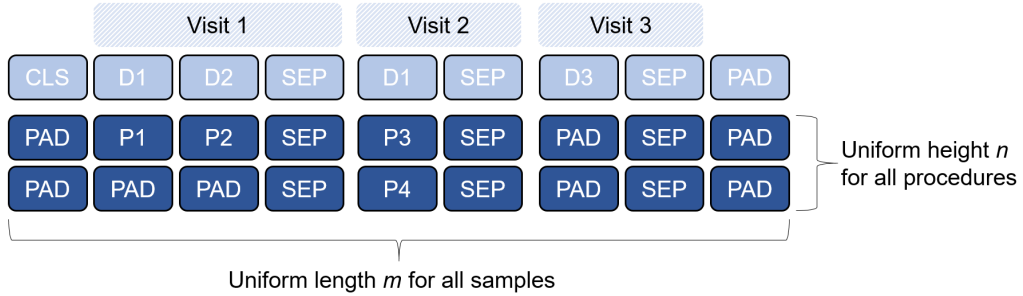


Figure 3: An example of how ExBEHRT represents the patient from figure 1. As the features are stacked vertically, additional concepts (such as labs as shown in figure 4) will not increase the sentence length m .

The padding token **PAD** can be understood as an indicator to the model which parts of a patient journey can be neglected, as they don't contain information. It is added at the end of a sentence to ensure the same length m for each patient. After the reshaping described above, all procedures of all patients are padded to the same amount of rows n to enable batch processing. n is set to the .95 percentile over all representations of visits of all patients before training. Since BMI, smoking status and gender naturally don't fluctuate within one visit, they do not need to be rearranged in a complex way. Therefore, the value recorded

within a visit is copied to all horizontal slots of the corresponding visit. In addition, the embeddings of diagnoses, age and segment are the same as described in the original BEHRT publication. Before the inputs are passed to the model, each token is embedded in a 288-dimensional vector and all tokens are summed vertically. A visualisation of the complete input can be found in Figure 4.

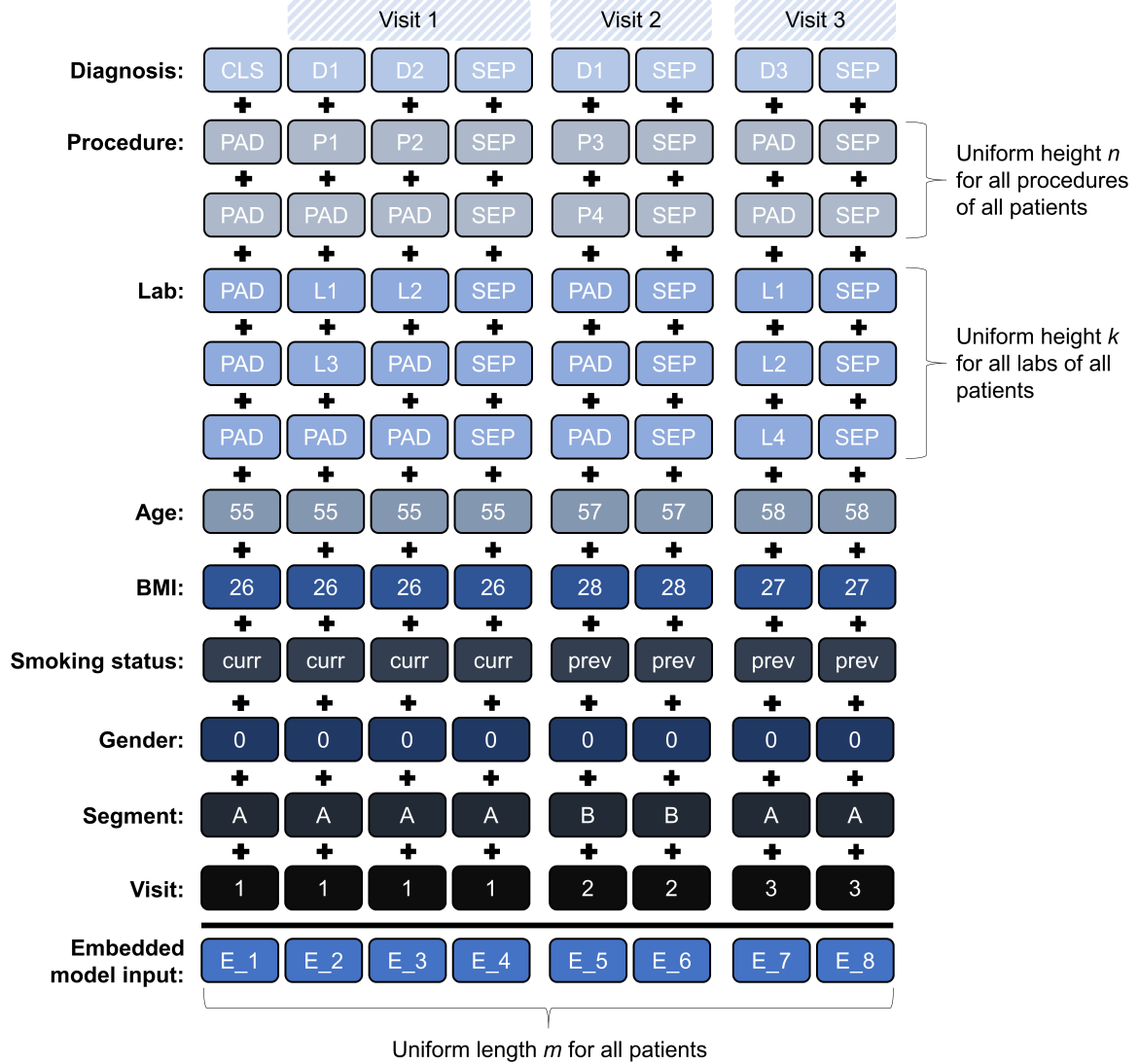


Figure 4: A sample input of ExBEHRT. Each of the concepts has its own embedding, where each of the tokens is mapped to a 288-dimensional vector, which is learned during model training. After embedding, all concepts are summed vertically element-wise to create a single $288 \times m$ dimensional vector as input for the model.

3.1. Pre-training with Masked Language Modelling

For pre-training the BERT-based models, we applied the standard MLM procedure described in the original BERT paper (Devlin et al. (2018)) applied on diagnosis code prediction using their BertAdam optimizer with cross-entropy loss. We followed the vast majority of subsequent papers, where in each iteration 15% of the diagnosis codes of a patient are selected randomly and either masked (80% of the time), replaced with another diagnosis code (10% of the time) or kept the same (10% of the time).

3.2. Fine-tuning on Disease-Specific Event Prediction

We validated our model on several disease-specific binary classification tasks from different domains. One oncology-specific task (Lu et al. (2022)) commonly found in the literature is the prediction of cancer patient mortality within six and twelve months. The observation window (the information provided to the model) is the entire patient journey to the first cancer diagnosis (including the visit with the first cancer diagnosis).

The third task, which was part of the CEHR-BERT paper, is to predict the readmission of a patient with heart failure to the hospital within 30 days after heart failure. The observation window includes all visits within one year before the (first) heart failure.

To account for the strong class imbalance between positive and negative outcomes, we also included focal loss (Lin et al. (2017)) in our hyperparameter search space. Focal loss reduces the relative loss for well-classified examples and puts more emphasis on difficult, misclassified examples.

3.3. Cancer Patient Clustering with ExBEHRT Embeddings

To generate patient clusters and visualize them in a meaningful way, we applied a combination of the dimensionality reduction technique UMAP (McInnes et al. (2018)) and the clustering algorithm HDBSCAN (Campello et al. (2013)). As ExBEHRT is not specialized on a specific disease, we conducted another pass of pre-training, where we initialized the model weights with the pre-trained ExBEHRT weights and applied MLM on cancer diagnosis codes only. This non-finetuned model was then used for generating the patient embeddings. After training, we conducted the following steps for the unsupervised clustering:

- a) Generate the ExBEHRT embedding (vector of size 288) for each patient (stemming from the CLS token at the beginning of each patient journey)
- b) Reduce the embeddings' size from *a*) from 288 to 10 using UMAP to get representations for clustering and avoid the curse of dimensionality
- c) Cluster the 10-dimensional vectors using HDBSCAN
- d) Reduce the embeddings' size from *a*) from 288 to 2 using UMAP to get 2D coordinates for each patient
- e) Visualize the Clusters from *c*) in the 2D space of the embedding from *d*)

4. Cohort

In this study, we used the Optum[®] de-identified EHR database. It is derived from health-care provider organizations in the United States, which include more than 57 contributing sources and 111,000 sites of care including hospital-based medical services networks comprising academic, private, and community hospitals treating more than 106 million patients. Optum[®] data elements also include demographics, medications prescribed and administered, immunizations, allergies, lab results (including microbiology), vital signs and other observable measurements, clinical and hospitalisation administrative data, and coded diagnoses and procedures. The population in Optum[®] EHR is geographically diverse, spanning all 50 US states.

4.1. Pre-Training Cohort

We selected only data points collected during hospitalisations to ensure the quality and consistency of the data². Each patient must have at least five visits with valid ICD-9 or ICD-10 diagnosis codes to ensure sufficient temporal context. Our cohort is selected with the same criteria as in BEHRT, resulting in 5.4M individuals. In order to prevent any sort of data leakage during pre-training and fine-tuning, the data is split into three datasets before training: training (80%), validation (10%) and testing (10%).

Table 1: Statistics of the pre-training cohort.

Feature	Metric
Birth year	1973 \pm 25, min: 1932, max: 2021
Gender	41.49% male, 58.51% female
Distribution by race	68% Cau., 22% Afr. Am., 1% As., 9% other
No. of diagnosis codes per patient	14 \pm 11.1, min: 5, max: 121
No. of visits per patient	9 \pm 6.6, min: 5, max: 63
% of patients without labs	14.33%
% of patients without procedures	1.64%
% of patients without BMI	21.74%
% of patients without smoking status	27.11%
% of deceased patients	14.52%

4.2. Fine-Tuning Cohorts

To validate the model’s performance on cancer-specific tasks, we limited patients to have at least five diagnoses, regardless of the number of visits, in order to incorporate enough information for valid predictions. At least one of these diagnoses must be a cancer code (ICD-10 C[0-99]). This cohort consists of 437,903 cancer patients (31.67% deceased within 6 months and 38.45% within 12 months of first cancer diagnosis), split into three datasets (training (80%), validation (10%), test (10%)), with each patient who is also part of the

2. This includes emergency patients, inpatients, observation patients, nursing facility patients, hospice patients and inpatient rehabilitation patients.

pre-training cohort described in section 4.1 being assigned to the same data split as in the other cohort to avoid data leakage.

We constructed the heart failure readmission cohort similarly, but did not restrict patients to a specific number of visits or diagnoses as long as one code was a heart failure code (ICD-10 I50). Again, we felt this was an appropriate use-case for clinicians. This resulted in a cohort of 503,161 heart failure patients (28.24% readmitted within 30 days), split into three data sets. The detailed statistics of these two cohorts can be found in the appendix 6.

4.3. Data Processing

For the diagnoses, we mapped all ICD-9 codes to ICD-10 codes according to the general equivalence mappings provided by the National Bureau of Economic Research³. Furthermore, only primary diagnoses are considered, as we wanted to focus on the most important diagnostics. Similar to Meng et al. (2021) and Choi et al. (2015), we limited the diagnosis codes to three characters to maintain a reasonable amount of relevant detail. Per visit diagnoses were de-duplicated to avoid biasing the model towards recurring codes during long visits. After de-duplication, patients with more than 128 diagnoses were discarded, as only 0.625% of all patients had more than 128 diagnosis codes. In addition, we included procedures⁴ and laboratory types⁵ in the model. As with diagnoses, procedure codes and laboratory types were de-duplicated per visit.

In addition to diagnoses, procedures, laboratory types, age and gender, we incorporated two of the least sparse observations in the dataset, which are empirically known to have high predictive power for disease trajectories: BMI and smoking status. If a value is missing for a particular visit, the last previous value is taken. Other observations with higher coverage such as pulse, body temperature and blood pressure were not taken into account, as they usually have a more granular influence on diseases.

5. Results

5.1. General Evaluation Approach

Besides different baseline transformer models (BEHRT and Med-BERT), we also trained a version of ExBEHRT on the two pre-training objectives (MLM + PLOS) proposed in the publication of Med-BERT (Rasmy et al. (2021)) to verify potential benefits of having a second pre-training objectives (referred to as ExBEHRT+P).

5.2. Pre-Training Results

For pre-training ExBEHRT, we used the hyperparameters and model architecture proposed by the BEHRT paper. To ensure a fair comparison, we used the same amount of attention layers (6) and heads (12) as well as embedding dimension (288) for all three BERT-based models. For BEHRT and Med-BERT, we used the implementation provided by the authors

3. <https://www.nber.org/research/data/icd-9-cm-and-icd-10-cm-and-icd-10-pcs-crosswalk-or-general-equivalence->

4. Optum[®] EHR defines procedures as medications as well as disease screenings, surgical procedures and other medical services.

5. Urinalysis, haematology, special chemistry, special laboratory, chemistry and blood gas

of the corresponding publications⁶. All models were trained for 40 epochs on a Tesla T4 GPU with 16GB memory, where, as in the original publication, the epoch with the highest micro-averaged MLM precision score⁷ was selected. We further report the balanced accuracy to get a better sense of the overall performance of the models.

Table 2: Pre-Training results of various models.

	BEHRT	Med-BERT	ExBEHRT	ExBEHRT+P
Precision	54.6%	56.2%	64.2%	63.9%
Balanced Accuracy	8.86%	8.03%	16.58%	15.52%

As presented in table 2, adding additional features to BEHRT significantly increases the pre-training performance in diagnosis code prediction. Adding a second pre-training objective slightly harms the MLM performance, but could nevertheless lead to improved fine-tuning performance due to additional context.

5.3. Fine-Tuning on Event Prediction Results

For this set of tasks we report the metrics commonly used to evaluate algorithms that perform binary predictions: area under the receiver operating characteristic curve (AUROC), average precision score (APS) and the precision at the 0.5 threshold. We used their micro-averaged implementations to follow the line of previous work and ensure a more robust assessment of the overall performance. More details on the hyperparameter optimization process can be found in appendix 6. We denote the task of prediction of death within N months after the first cancer prediction as *Death in 6M* and *Death in 12M* and predicting readmission of patients within 30 days of their first heart attack as *HF readmit*.

In addition to comparing the performance of our algorithm with that of BEHRT, we also benchmarked against two of the best performing "conventional" machine learning algorithms for tabular data, XGBoost (XGB, [Chen and Guestrin \(2016\)](#)) and Logistic Regression (LR). Details on the preprocessing of the data and the tuning of the hyperparameters can be found in appendix 6.

Table 3: Average fine-tuning results of various models and their standard deviations.

Task	Metric	LR	XGB	BEHRT	Med-BERT	ExBEHRT	ExBEHRT+P
Death in 6M	APS	42.8±0.0%	45.5±0.1%	47.7±0.4%	46.2±0.4%	53.1±0.3%	52.6±0.3%
	AUROC	63.5±0.0%	66.4±0.1%	66.7±0.6%	65.3±0.3%	71.5±0.5%	70.9±0.5%
	Precision	73.0±0.1%	74.3±0.1%	75.2±0.2%	74.5±0.1%	78.1±0.1%	77.9±0.1%
Death in 12M	APS	51.6±0.0%	45.5±0.1%	55.5±0.1%	54.4±0.2%	59.8±0.2%	59.6±0.2%
	AUROC	66.7±0.0%	66.3±0.1%	70.1±0.2%	68.9±0.3%	74.3±0.4%	73.8±0.4%
	Precision	70.4±0.1%	74.4±0.1%	73.2±0.1%	72.4±0.1%	76.4±0.1%	76.3±0.1%
HF readmit	APS	29.8±0.0%	31.3±0.1%	19.9±0.1%	19.8±0.1%	30.0±1.6%	25.1±0.1%
	AUROC	51.9±0.1%	53.6±0.1%	51.2±0.1%	51.0±0.1%	56.7±1.7%	56.8±0.2%
	Precision	72.0±0.0%	72.3±0.1%	81.0±0.1%	81.0±0.0%	78.7±0.2%	81.6±0.1%

6. The source code can be found here: <https://github.com/deepmedicine/BEHRT> and <https://github.com/ZhiGroup/Med-BERT>

7. Per default, the precision score is evaluated at a 0.5 threshold. Certainly, one could apply additional model calibration, but we hypothesized that this could introduce bias before fine-tuning.

As shown in table 3, the variants of ExBEHRT outperform the four baselines we created on all tasks. We also found that the addition of the second pre-training target PLOS can lead to slightly better performance in some scenarios, but is not superior overall. Nonetheless, XGBoost provides a higher APS than the transformer-based models on HF Readmit, but performs worse on the other metrics.

For the two cancer mortality tasks, we further performed a cancer-specific evaluation of the ten most common cancers, as the different cancer types differ drastically in their expected outcomes. This evaluation can be found in appendix 6. For all tasks presented here, we also examined the effects of omitting certain concepts to measure the impact of the new features. These ablations can be found in appendix 6. In addition, we examined the effects on the positional variance of concepts within a visit. Since the model was trained to predict diagnosis codes at specific time points and not within a visit, there could be a possible bias that the model performs worse when the different features are mixed within a visit. The model should perform similarly regardless of which slot procedures and laboratory values are added to, as there is no temporal order within a visit. This ablation can be found in appendix 6.

5.4. Interpretability on Event Prediction Results

For all interpretability experiments, we used the ExBEHRT model fine-tuned on the task *Death in 6M*, meaning whether a cancer patient will decrease within six months after their first cancer diagnosis. We visualize the interpretability for individual patients only, as both interpretability approaches presented here are example-based and not model-agnostic.

5.4.1. SELF-ATTENTION VISUALIZATION

Analogous to previous work (Li et al. (2020), Rasmy et al. (2021), Meng et al. (2021)), we visualised the attention of the last network layer using BertViz (Vig (2019)). However, since in all of these models the embeddings are summed before being passed through the network, self-attention has no way of attributing individual input features to the outcome. Nevertheless, we can draw conclusions about how the different slots interact with each other and which connections the model considers important. Figure 5 shows the self-attention of a single patient in the last layer of ExBEHRT. The journey represents a 69-year-old woman who never smoked and died a year after being diagnosed with lung cancer. The left figure shows the attention of all 12 attention heads in this layer, while the right figure shows the attention of one single head. As expected, the model focuses heavily on the slots within a visit, as these slots are highly interconnected by definition. Although the model was not specifically trained on cancer codes, it pays close attention to slot 7 (slot containing the cancer diagnosis), suggesting that it has learned some correlation between the cancer diagnosis and the predicted outcome. Interestingly, slot 7 receives a lot of attention on the first and second visits, but not on the other two previous visits, suggesting that the model is able to learn causality over long periods of time. Table 15 in appendix 6 contains information about all diagnoses, procedures and labs for each slot of the patient from the figure 5.

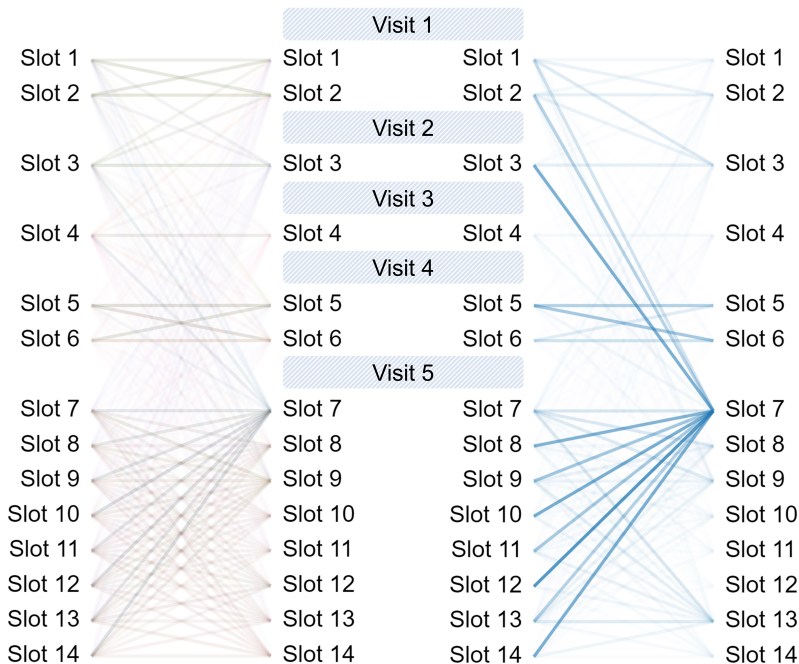


Figure 5: Left: The self-attention of all 12 attention heads of the last layer of ExBEHRT. Higher opacity corresponds to higher attention. Right: The self-attention of one attention head of the last layer.

5.4.2. EXPECTED GRADIENTS INTERPRETABILITY

Due to the limitations of self-attention visualisation, we have explored the technique Expected Gradients (Erion et al., 2020) for more detailed interpretability. With this algorithm, we can infer the meaning of individual input tokens, which is not possible with self-attention. Since each token (diagnosis code, procedure code, age, etc.) is mapped to a 288-dimensional embedding before being passed to the model, we first calculated the expected gradients for the embedding and then summed the absolute values to obtain a single gradient value for each token. In this way, each individual token has an associated gradient that is linked to the output of the model and provides detailed insights into which medical concept has what impact on the prediction of the model. Our example patient is a 58-year-old woman who was a regular smoker. She died at the age of 65, three months after her blood cancer diagnosis. In figure 6, we summed all expected gradients for each of the input features. This way, we can evaluate the feature importances on the output for a specific patient. For this patient, diagnoses and procedures (treatments & medications) were by far the most importance features. With this visualization, we can further evaluate basic biases. For example, gender was not considered to be an important feature, indicating that predictions would be similar for a person with another gender.

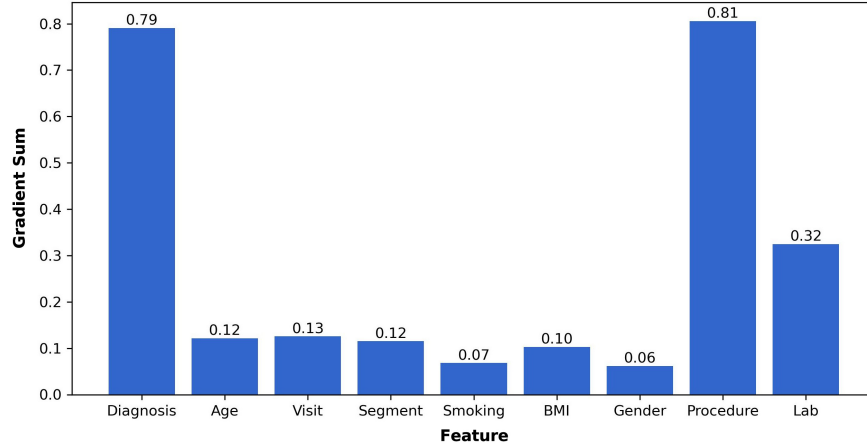


Figure 6: The absolute sums of the expected gradients summed by input feature.

In figure 7, we visualized the absolute expected gradients for each of the features and summed them at each time slot. This way, we can evaluate the different feature importances over time to get a notion of where the model puts emphasis on. Interestingly, the model put more importance on what kind of medications & treatments that patient received in the first two visits, where as in the last visit (the visit in which the patient was diagnosed with blood cancer), it put more importance on diagnoses and labs. Generally, slot 5, where the cancer was diagnosed, was attributed with the highest importance.

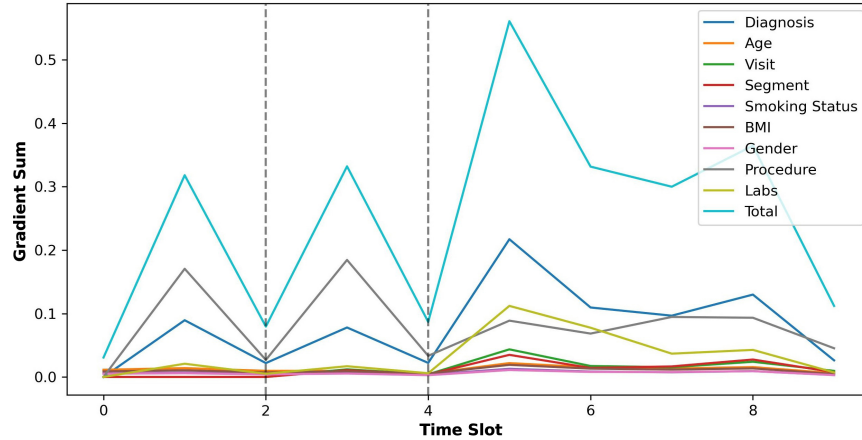


Figure 7: The absolute sums of the expected gradients summed by input feature and time slot. The dotted lines indicate the next visit.

Figure 8 displays the absolute sums of gradients of each individual input token, providing a detailed interpretation of which medical concept has had what impact on the models prediction. Unsurprisingly, the cancer code C81 has had the biggest impact on the outcome. However, earlier codes like J40 or 71020 also contribute to the models prediction, indicating that the model includes information from the whole patient journey into its predictions.

Diagnosis										
CLS	J40	SEP	M54	SEP	C81	R55	R59	E87	SEP	
Lab	-	-	-	-	-	CHEMISTRY	URINALYSIS	HEMATOLOGY	SPEC. CHEM.	-
	-	-	-	-	-	SPEC. LAB	BLOOD GAS	-	-	-
Procedure										
-	71020	-	81003	-	-	-	-	-	-	-
-	94640	-	87077	-	-	-	-	-	-	-
-	99283	-	87086	-	-	-	-	-	-	-

Figure 8: A visualization of the absolute sums of the expected gradients of diagnoses, labs and procedures on a concept level. Darker colours represent higher values and the SEP tokens indicate the separation between two visits.

5.5. Patient Clustering

From the 260'645 cancer patients from the general cohort, HDBSCAN was able to cluster 90% (234'575) into 24 clusters (mean: 9'774, min: 1'102, max: 47'722). As shown in figure 9, the clusters are clearly separated spatially, indicating a distinct separation of the different cancer types. We labelled each cluster with the most occurring diagnosis code within this cluster, regardless of the type of code. Interestingly, similar concepts (e.g. cancer of female reproductive organs (clusters 14-16), different types of leukaemia (clusters 6-8)) or cancer of digestive organs (clusters 2, 4, 5, 18, 19) lay in areas close to each other, indicating a spatial logic within the disease types.

On average, the most common cancer diagnosis within a cluster was present in 84% of patients assigned to that cluster, indicating a strong internal focus on cancer codes within the model. Of the 23 clusters, 22 had a unique cancer code as the most common diagnosis and included, on average, 85% of all patients diagnosed with the corresponding cancer code. These two metrics indicate strong cross-cluster purity and homogeneity within the clusters. For a more detailed description of all clusters as well as the hyperparameters used in the different clustering steps, see appendix 6 in table 14 and figures 13 and 14.

5.5.1. DISEASE SUBTYPING

To draw conclusions about the internal clustering of HDBSCAN, we examined the most frequently occurring diagnoses, procedures and labs for each cluster. We focused only on concepts that occurred at least 5% more frequently within the cluster than in the entire cohort. In this way, we ensured that very common diagnoses such as pelvic pain were not included in our cluster analysis.

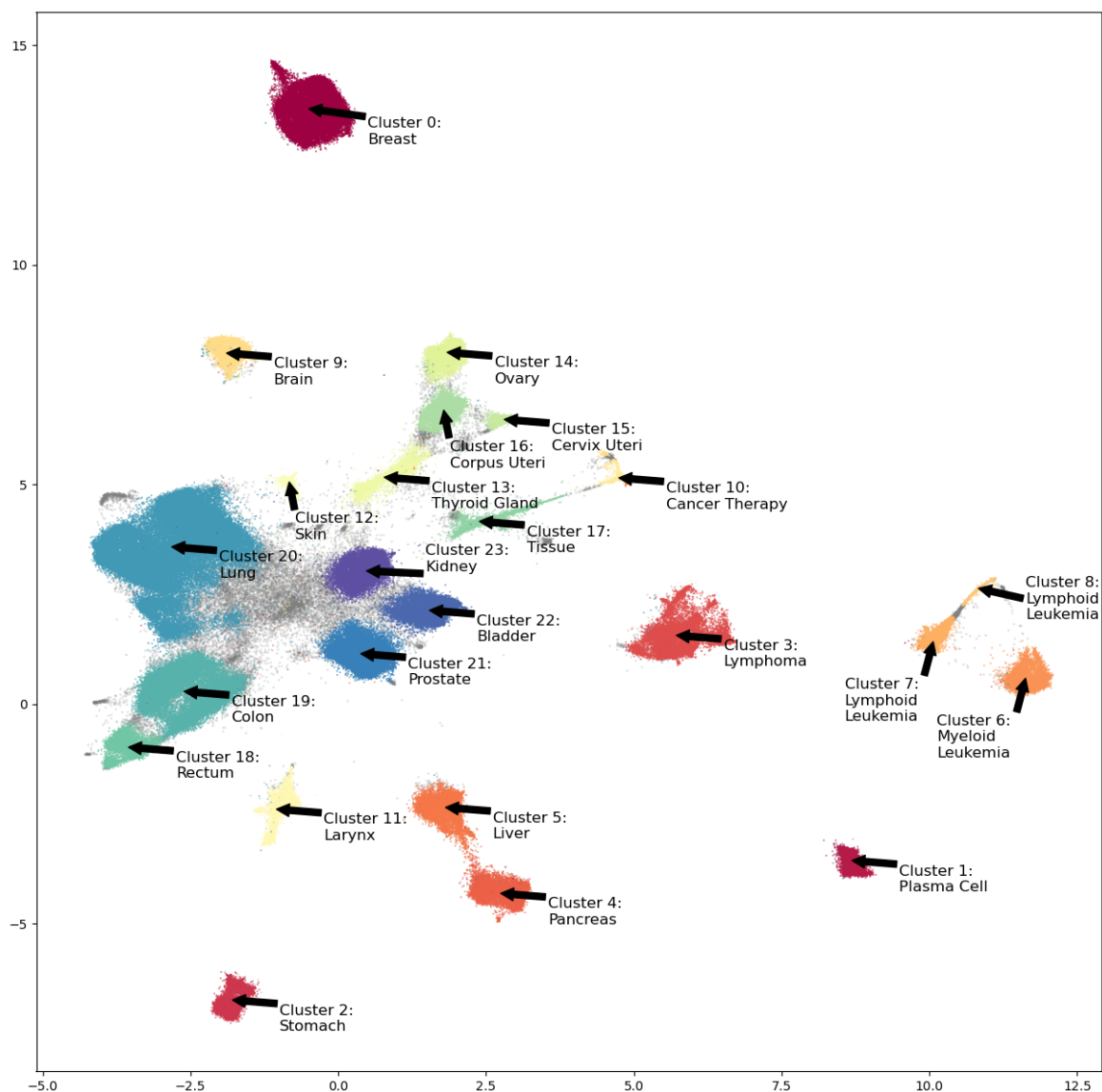


Figure 9: The unsupervised cluster assignments from HDBSCAN, visualized with a 2-dimensional UMAP projection. The gray points are patients not assigned to any cluster (10%). The labels indicate the most frequent diagnosis code of each cluster. Besides cluster 10, all labels are neoplasms.

A closer look at clusters 7 and 8 shows the potential of ExBEHRT to form subgroups of the same cancer type (Figures 10 & 11). Although almost all patients in both clusters have lymphocytic leukaemia, their diagnoses, procedures and applied laboratory tests differ considerably.

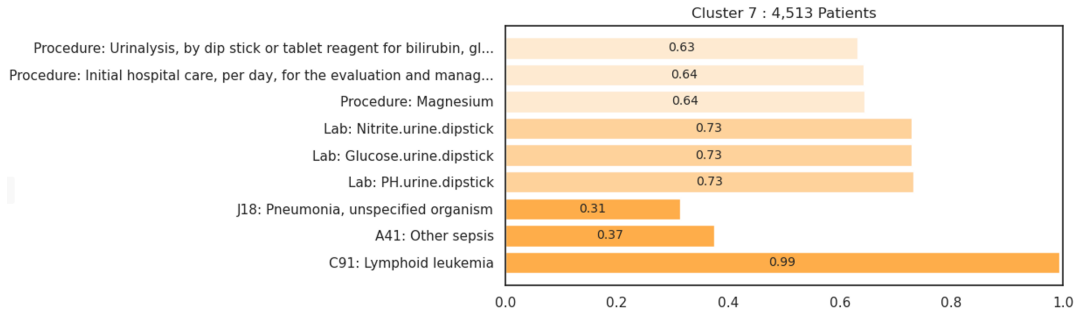


Figure 10: The three most common procedures, labs and diagnoses for the CLL cluster.

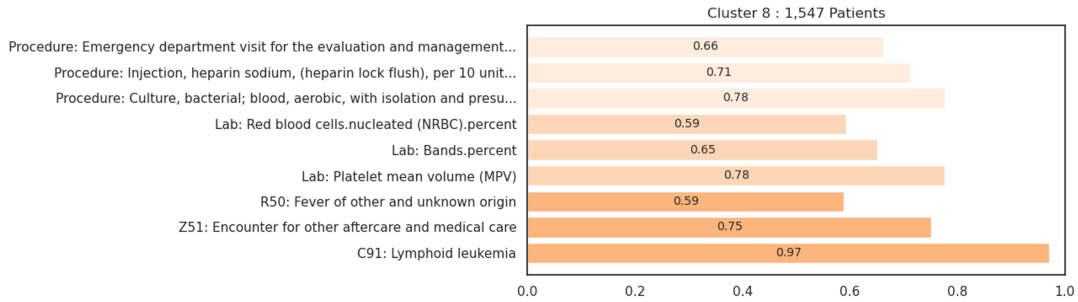


Figure 11: The three most common procedures, labs and diagnoses for the ALL cluster.

Examination of the different patient characteristics (table 4) of these two clusters (table 4) shows that the model has indeed learned to distinguish between chronic lymphocytic leukaemia (CLL, cluster 7) and acute lymphocytic leukaemia (ALL, cluster 8) without having explicit information on these subtypes. As we limited the ICD-10 codes to three digits, only the general lymphocytic leukemia code C91 is given to the model without the subtypes C91.0 for ALL and C91.1 for CLL. In the table, *% of journey with cancer* indicates the ratio of the time between the first and last cancer diagnosis compared to the duration of the whole patient journey. *Cancer-free* refers to the percentage of patients within a cluster, which have records of at least two visits after the last visit with a cancer diagnosis. The *average death rate* comes directly from the Optum[®] EHR database and unfortunately does not indicate the cause of death.

Table 4: Statistics of the two lymphoblastic leukemia clusters indicating a clear separation between CLL and ALL.

Metric	Cluster 7 (CLL)	Cluster 8 (ALL)
Median age	70	5
Median birth year	1946	2009
Median BMI	26	17
% of men	60.5%	55.2%
Average death rate	54.7%	6.6%
% of journey with cancer	29.9%	45.5%
Cancer-free	47.3%	48.1%

Another example, the pancreatic cancer cluster 4, shows that with a second pass of HDBSCAN on this cluster only, we can identify risk subgroups of pancreatic cancer. In all three identified clusters, more than 90% of the patients actually do have pancreatic cancer and all share similar general characteristics.

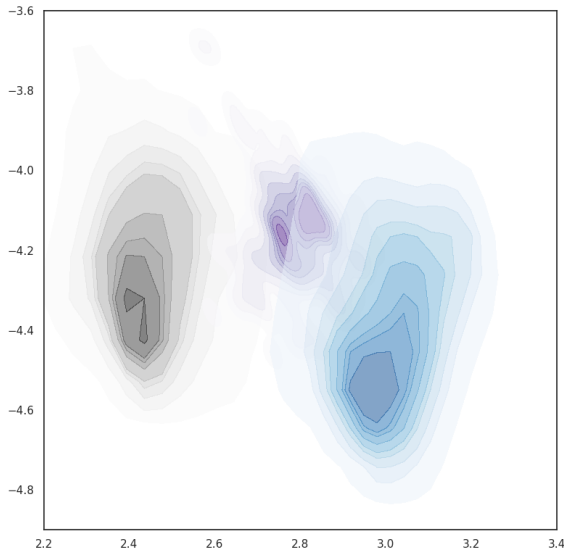


Figure 12: The three identified patient subclusters with pancreatic cancer visualized with a kernel density estimate plot for visual clarity. Even though the three clusters generally share the same characteristics in diagnoses, Age, BMI etc., patients belonging to the smaller purple cluster died less frequently and recovered nearly twice as often from cancer compared to the other two clusters.

However, as displayed in table 5, ExBEHRT identified one subgroup with significantly higher chance of recovering from cancer and a lower probability of death, even though this information was not provided to the model at any point.

Table 5: Statistics of the three pancreatic cancer clusters indicating a clear differentiation between higher risk (gray, blue) and lower risk patients (purple).

Metric	Gray	Blue	Purple
Median age	67	68	68
Median birth year	1950	1947	1944
Median BMI	25	25	26
% of men	52.3%	50.9%	60.0%
Average death rate	76.5%	75.9%	70.0%
% of journey with cancer	27.0%	24.0%	18.3%
Cancer-free	34.0%	36.9%	62.7%

6. Discussion

In this study, we presented a novel method for adding patient features to BEHRT that significantly increases the predictive power for multiple downstream tasks in different disease domains. The novel method of stacking features vertically led to improvements in hardware requirements and benchmarks, and facilitates the possible extension to new concepts in the future. Given the large number and heterogeneity of patients with which the model was pre-trained, we are confident that ExBEHRT will generalise well to new data, patients and tasks. Combined with interpretability, the model offers more detailed insights into disease trajectories and subtypes of different patients than previous approaches, which could help clinicians form more detailed assessments of their patients’ course and health. Furthermore, with a personalised understanding of patient groups, it is possible to identify unmet needs and improve patient outcomes.

Limitations and Future Work

It is worth noting that the pre-training precision reported in BEHRT’s original paper is higher than the one we were able to reproduce with the same model on our data (0.6597 (theirs) vs. 0.5456 (ours)). One possible explanation is that we drastically increased the task complexity since our model predicts a label out of 1916 instead of 300 diagnosis concepts. Nevertheless, we were able to show that additional features significantly improved both the quantitative and qualitative performance of the model, and we expect that this would also be the case when using the original dataset and the medical codes from BEHRT. Furthermore, it is extremely difficult to validate the quality, completeness and correctness of EHR datasets because EHR data is usually processed anonymously and comes from a variety of heterogeneous, fragmented sources. The pure nature of EHR data also introduces bias, as physicians may have an incentive to diagnose additional or other conditions, as medical billing is closely related to the number and type of diagnoses reported.

In addition, there is also the question of bias and fairness in our results. In a possible next step, we would like to verify the results and interpretations of this work with clinicians to ensure robust and sound predictions given the interpretability we have acquired. In addition, we would like to test the generalisability of ExBEHRT to other clinical use-cases such as severity prediction and risk typing of other diseases and certain cancers.

References

- Takuya Akiba, Shotaro Sano, Toshihiko Yanase, Takeru Ohta, and Masanori Koyama. Optuna: A next-generation hyperparameter optimization framework. *KDD 2019 Applied Data Science track*, 7 2019.
- Alaleh Azhir, Soheila Talebi, Louis-Henri Merino, Yikuan Li, Thomas Lukasiewicz, Edgar Argulian, Jagat Narula, and Borislava Mihaylova. Behrtday: Dynamic mortality risk prediction using time-variant covid-19 patient specific trajectories. *AMIA Annu Symp Proc*, 2022.
- Tom B. Brown, Benjamin Mann, Nick Ryder, Melanie Subbiah, Jared Kaplan, Prafulla Dhariwal, Arvind Neelakantan, Pranav Shyam, Girish Sastry, Amanda Askell, Sandhini

- Agarwal, Ariel Herbert-Voss, Gretchen Krueger, Tom Henighan, Rewon Child, Aditya Ramesh, Daniel M. Ziegler, Jeffrey Wu, Clemens Winter, Christopher Hesse, Mark Chen, Eric Sigler, Mateusz Litwin, Scott Gray, Benjamin Chess, Jack Clark, Christopher Berner, Sam McCandlish, Alec Radford, Ilya Sutskever, and Dario Amodei. Language models are few-shot learners. *NIPS*, 5 2020.
- Ricardo J G B Campello, Davoud Moulavi, and Joerg Sander. Density-based clustering based on hierarchical density estimates. *Advances in Knowledge Discovery and Data Mining*, 2013.
- Tianqi Chen and Carlos Guestrin. Xgboost: A scalable tree boosting system. *KDD*, 3 2016.
- Edward Choi, Mohammad Taha Bahadori, Andy Schuetz, Walter F. Stewart, and Jimeng Sun. Doctor ai: Predicting clinical events via recurrent neural networks. *Machine Learning and Healthcare Conference*, 11 2015.
- Jacob Devlin, Ming-Wei Chang, Kenton Lee, and Kristina Toutanova. Bert: Pre-training of deep bidirectional transformers for language understanding. *ACL*, 10 2018.
- Gabriel Erion, Joseph D Janizek, Pascal Sturmfels, Scott M Lundberg, Su-In Lee, and Paul G Allen. Improving performance of deep learning models with axiomatic attribution priors and expected gradients. *Nature*, 2020.
- Katikapalli Subramanyam Kalyan, Ajit Rajasekharan, and Sivanesan Sangeetha. Ammu: A survey of transformer-based biomedical pretrained language models. *Journal of Biomedical Informatics*, 2 2022.
- Yikuan Li, Shishir Rao, José Roberto Ayala Solares, Abdelaali Hassaine, Rema Ramakrishnan, Dexter Canoy, Yajie Zhu, Kazem Rahimi, and Gholamreza Salimi-Khorshidi. Behrt: Transformer for electronic health records. *Nature*, 2020.
- Yikuan Li, Mohammad Mamouei, Gholamreza Salimi-Khorshidi, Shishir Rao, Abdelaali Hassaine, Dexter Canoy, Thomas Lukasiewicz, and Kazem Rahimi. Hi-behrt: Hierarchical transformer-based model for accurate prediction of clinical events using multimodal longitudinal electronic health records. *Journal of Biomedical and Health Informatics*, 2021.
- Tsung Yi Lin, Priya Goyal, Ross Girshick, Kaiming He, and Piotr Dollar. Focal loss for dense object detection. *IEEE*, 8 2017.
- Sheng Chieh Lu, Cai Xu, Chandler H. Nguyen, Yimin Geng, André Pfob, and Chris Sidey-Gibbons. Machine learning-based short-term mortality prediction models for patients with cancer using electronic health record data: Systematic review and critical appraisal. *Journal of Medical Internet Research*, 3 2022.
- Leland McInnes, John Healy, and James Melville. Umap: Uniform manifold approximation and projection for dimension reduction. *The Journal of Open Source Software*, 2 2018.

- Yiwen Meng, William Speier, Michael K. Ong, and Corey W. Arnold. Bidirectional representation learning from transformers using multimodal electronic health record data to predict depression. *Journal of Biomedical and Health Informatics*, 8 2021.
- Chao Pang, Xinzhuo Jiang, Krishna S Kalluri, Matthew Spotnitz, RuiJun Chen, Adler Perotte, and Karthik Natarajan. Cehr-bert: Incorporating temporal information from structured ehr data to improve prediction tasks. *Proceedings of Machine Learning for Health*, 11 2021.
- Raphael Poulain, Mehak Gupta, and Rahmatollah Beheshti. Few-shot learning with semi-supervised transformers for electronic health records. *Proceedings of Machine Learning Research*, 182, 2022.
- Pks Prakash, Srinivas Chilukuri, Nikhil Ranade, and Shankar Viswanathan. Rarebert: Transformer architecture for rare disease patient identification using administrative claims. *Proceedings of the AAAI Conference on Artificial Intelligence*, 2021.
- Shishir Rao, Mohammad Mamouei, Gholamreza Salimi-Khorshidi, Yikuan Li, Rema Ramakrishnan, Abdelaali Hassaine, Dexter Canoy, and Kazem Rahimi. Targeted-behrt: Deep learning for observational causal inference on longitudinal electronic health records. *IEEE*, 2022.
- Laila Rasmy, Yang Xiang, Ziqian Xie, Cui Tao, and Degui Zhi. Med-bert: pre-trained contextualized embeddings on large-scale structured electronic health records for disease prediction. *Nature*, 2021.
- Junyuan Shang, Tengfei Ma, Cao Xiao, and Jimeng Sun. Pre-training of graph augmented transformers for medication recommendation. *International Joint Conferences on Artificial Intelligence*, 6 2019.
- Jesse Vig. A multiscale visualization of attention in the transformer model. *ACL*, 2019.

Appendix A. Fine-Tuning Cohorts

Table 6: Statistics of the cohort used for mortality prediction within six and twelve months after first cancer diagnosis.

Feature	Metric
Cohort Size	437'903
Birth year	1951 \pm 15, min: 1932, max: 2021
Gender	50.42% male, 49.58% female
Distribution by race	68% Cau., 22% Afr. Am., 1% As., 9% other
No. of diagnosis codes per patient	15 \pm 12.6, min: 5, max: 118
No. of visits per patient	7 \pm 6.1, min: 1, max: 63
% of patients with outcome 6M	31.67%
% of patients with outcome 12M	38.45%
% of patients without labs	18.81%
% of patients without procedures	1.57%
% of patients without BMI	21.83%
% of patients without smoking status	29.11%
% of deceased patients	54.61%

Table 7: Statistics of the cohort used readmission prediction after heart failure within 30 days.

Feature	Metric
Cohort Size	503'161
Birth year	1945 \pm 14, min: 1932, max: 2021
Gender	51.81% male, 48.19% female
Distribution by race	77% Cau., 16% Afr. Am., 1% As., 6% other
No. of diagnosis codes per patient	18 \pm 16.4, min: 1, max: 123
No. of visits per patient	8 \pm 7.9, min: 1, max: 63
% of patients with outcome	28.24%
% of patients without labs	20.49%
% of patients without procedures	2.56%
% of patients without BMI	23.91%
% of patients without smoking status	30.36%
% of deceased patients	51.63%

Appendix B. Fine-Tuning Model Details

BEHRT Hyperparameter Selection

In order to tune the hyperparameters for downstream tasks, we applied a grid-search over the following parameters, selected the model with the best validation set performance and only then reported the performance on the test set:

- Learning rate: $3e-5$, $4e-5$, $5e-5$
- Loss function: Cross-entropy, focal loss ($\gamma = 2$), focal loss ($\gamma = 5$), focal loss ($\gamma = 2$, $\alpha = 0.75$)
- Optimizer warmup: No warmup, warmup (warmup proportion=0.1, weight decay=0.01)

Table 8: Fine-tuning hyperparameters on event prediction results of the BERT-based models.

		BEHRT	Med-BERT	ExBEHRT	ExBEHRT+P
Death in 6M	LR	$5e-5$	$5e-5$	$5e-5$	$5e-5$
	Loss	focal ($\gamma = 2$)	focal ($\gamma = 2$)	focal ($\gamma = 5$)	focal ($\gamma = 5$)
	Warmup	yes	no	no	yes
Death in 12M	LR	$5e-5$	$5e-5$	$5e-5$	$5e-5$
	Loss	focal ($\gamma = 2$)	focal ($\gamma = 5$)	focal ($\gamma = 5$)	focal ($\gamma = 5$)
	Warmup	yes	no	no	no
HF readmit	LR	$5e-5$	$5e-5$	$5e-5$	$5e-5$
	Loss	focal ($\gamma = 5$)	focal ($\gamma = 5$)	cross-entropy	focal ($\gamma = 5$)
	Warmup	yes	no	yes	yes

Conventional Models Data Pre-Processing & Hyperparameter Selection

To establish a baseline for the event prediction tasks, we conducted experiments with XGBoost and Logistic Regression, two versatile machine learning algorithms for tabular data. For data pre-processing, we ensured that the models had the same information as the transformer-based approaches. For the cancer patient mortality prediction, this means the entire journey to the first cancer prediction, and for the readmission tasks, a time window of one year to the first heart failure. Since neither model can work with time-series data, we converted the patient journeys into multi-hot encoded features, with each column indicating whether and how often the patient was assigned a particular diagnosis, procedure or laboratory. We also included a one-hot-coded vector for smoking status, a column for number of visits, gender, and a patient’s last and first BMI value and age. In this way, we wanted to ensure a fair comparison, as the models can access the same set of variables as ExBEHRT.

To tune the hyperparameters, we used the library Optuna ([Akiba et al. \(2019\)](#)), a renowned hyperparameter optimization framework and optimized the mean-squared error while optimizing the following parameters for XGB: learning rate (LR), maximum tree depth (max_depth), number of estimators (n_estimators), column sampling by tree (colsample), row subsampling (subsample) and the regulation parameter α .

Table 9: The best XGBoost hyperparameters found by Optuna for the fine-tuning prediction tasks.

	LR	max_depth	n_estimators	colsample	subsample	α
Death in 6M	0.0729	12	538	0.8095	0.8119	0.1989
Death in 12M	0.1180	8	666	0.3705	0.7091	0.7988
HF readmit	0.0127	19	1148	0.4438	0.9937	0.5952

We conducted a similar hyperparameter search for logistic regression with the following parameters: class weight (balanced or none), the equation solver (Newton-Cholesky, Sag or Saga), and the two regularization parameters penalty and C.

Table 10: The best Logistic Regression hyperparameters found by Optuna for the fine-tuning prediction tasks.

	Class weight	Solver	Penalty	C
Death in 6M	None	Sag	L2	186.8192
Death in 12M	None	Saga	None	141.8034
HF readmit	None	Newton-Cholesky	None	162.0031

Appendix C. Fine-Tuning Cancer-Wise Evaluation

Since different cancer types empirically have highly varying predicted outcomes, we evaluated the model performance on the ten most common cancer types in the test dataset to spot potential bias.

Even though labels are heavily imbalanced for some cancer types and frequencies vary drastically, the model is able to perform well on the individual cancer subgroups and we couldn't identify a bias towards certain subgroups.

Table 11: The AUROC scores of ExBEHRT for the ten most common cancer types in the test dataset.

ICD-10	#Patients with code	Cancer description	%Patients with outcome 6M	ROCAUC Death in 6M	%Patients with outcome 12M	ROCAUC Death in 12M
C34	7312	Bronchus and lung	44.46%	0.7186	52.38%	0.7172
C18	3710	Colon	21.4%	0.6652	26.95%	0.6960
C50	2924	Breast	20.11%	0.7031	24.66%	0.7257
C61	2057	Prostate	17.36%	0.7255	21.78%	0.785
C25	1986	Pancreas	48.59%	0.7058	58.51%	0.6873
C80	1965	No specification of site	54.4%	0.7064	61.58%	0.6840
C64	1880	Kidney, except renal pelvis	16.76%	0.6824	20.96%	0.7336
C71	1760	Brain	30.06%	0.6789	40.06%	0.7111
C22	1594	Liver	49.18%	0.6989	54.83%	0.7123
C67	1472	Bladder	27.17%	0.6775	33.97%	0.7117

Appendix D. Ablations

Feature Ablations

Here, we conducted ablations on which features independently yields the biggest improvement on the three proposed fine-tuning tasks. Generally, adding procedures yields the most significant performance boost. Nevertheless, combining all features yields to the best performance for all but one metric in one task (Precision for *HF readmit*).

Table 12: Ablations on fine-tuning on event prediction results of our ExBEHRT model trained with different features starting with BEHRT (Diagnosis + Age + Segment + Visit), adding only procedures, only labs and only observations (BMI, smoking status, gender).

Task	Metric	BEHRT	BEHRT + Procedures	BEHRT + Labs	BEHRT + Observations	ExBEHRT
Death in 6M	APS	0.4778	0.5206	0.4786	0.4871	0.5312
	AUROC	0.6674	0.7034	0.6696	0.6791	0.7154
	Precision	0.7520	0.7762	0.7527	0.7566	0.7811
Death in 12M	APS	0.5545	0.5938	0.5566	0.5609	0.5978
	AUROC	0.7010	0.7352	0.7040	0.7063	0.7432
	Precision	0.7319	0.7611	0.7333	0.7369	0.7639
HF readmit	APS	0.1994	0.2412	0.1998	0.1994	0.2966
	AUROC	0.5117	0.5582	0.5117	0.5115	0.5677
	Precision	0.8102	0.8145	0.8106	0.8103	0.7873

Visit Shuffle Ablations

For these ablations, we randomly shuffled the diagnoses, procedures and labs within each visit of 50 random patients from the test dataset a total of 50 times. All other characteristics are time-dependent, as they also show changes within a visit, and were therefore excluded from shuffling. We followed the same principle for all three fine-tuning tasks to check for positional invariance within each visit. To determine the label purity for a patient, we divided the amount of the most frequently predicted label of $\{0.1\}$ by 50. A value of 1.0

would mean that the model predicted the same label on every shuffle, indicating positional invariance. We then took the mean of all 50 patients to determine the predicted label purity.

Table 13: The predicted label purity of the best-performing ExBEHRT models on all three subtasks.

Task	Aggregated Label Purity
Death in 6M	0.9820 \pm 0.05
Death in 12M	0.9884 \pm 0.06
HF readmit	0.9910 \pm 0.07

As shown in table 13, the purity on each task is very close to 1.0, indicating that the model is very robust regarding the in-visit order of diagnoses, procedures and labs and doesn’t put significant focus on it.

Appendix E. Clustering Details

Clustering Hyperparameters

The hyperparameters for the procedure of the clustering from section 3.3 were set as follows:

- UMAP for 10D representations (step *b*):
 - Size of local neighbourhood: 100
 - Minimum distance apart : 0.0
 - Distance metric: euclidean
- HDBSCAN clustering of the 10D representations (step *c*):
 - Minimum cluster size: 1000
 - Minimum samples: 1000
- UMAP for 2D representations (step *d*):
 - Size of local neighbourhood: 100
 - Minimum distance apart: 0.0
 - Distance metric: euclidean

Clustering Results

Table 14: Statistics of the different clusters of cancer patients. The in-cluster percentage indicates how many patients within the cluster were diagnosed with the most occurring code of this cluster. The purity percentage indicates how many of the patients diagnosed with the most occurring code were actually assigned to the indicated cluster. Cluster 10 was excluded as it is not a cancer cluster.

Cluster	Patients	Most occurring code	In-cluster	Purity
Cluster 0	22'053	C50	98%	98%
Cluster 1	6'248	C90	99%	94%
Cluster 2	8'250	C16	58%	93%
Cluster 3	14'565	C85	54%	89%
Cluster 4	10'642	C25	95%	95%
Cluster 5	9'377	C22	80%	88%
Cluster 6	7'263	C92	88%	92%
Cluster 7	4'513	C91	99%	67%
Cluster 8	1'547	C91	97%	22%
Cluster 9	6'815	C71	95%	83%
Cluster 11	7'399	C32	32%	94%
Cluster 12	1'847	C43	99%	89%
Cluster 13	5'458	C73	66%	87%
Cluster 14	6'668	C56	93%	92%
Cluster 15	2'174	C53	99%	85%
Cluster 16	6'870	C54	85%	90%
Cluster 17	3'705	C49	70%	71%
Cluster 18	7'387	C20	87%	89%
Cluster 19	20'772	C18	82%	86%
Cluster 20	47'722	C34	77%	93%
Cluster 21	13'119	C61	93%	90%
Cluster 22	9'679	C67	92%	90%
Cluster 23	9'400	C64	93%	83%
Total	233'473	-	84%	85%

ExBEHRT

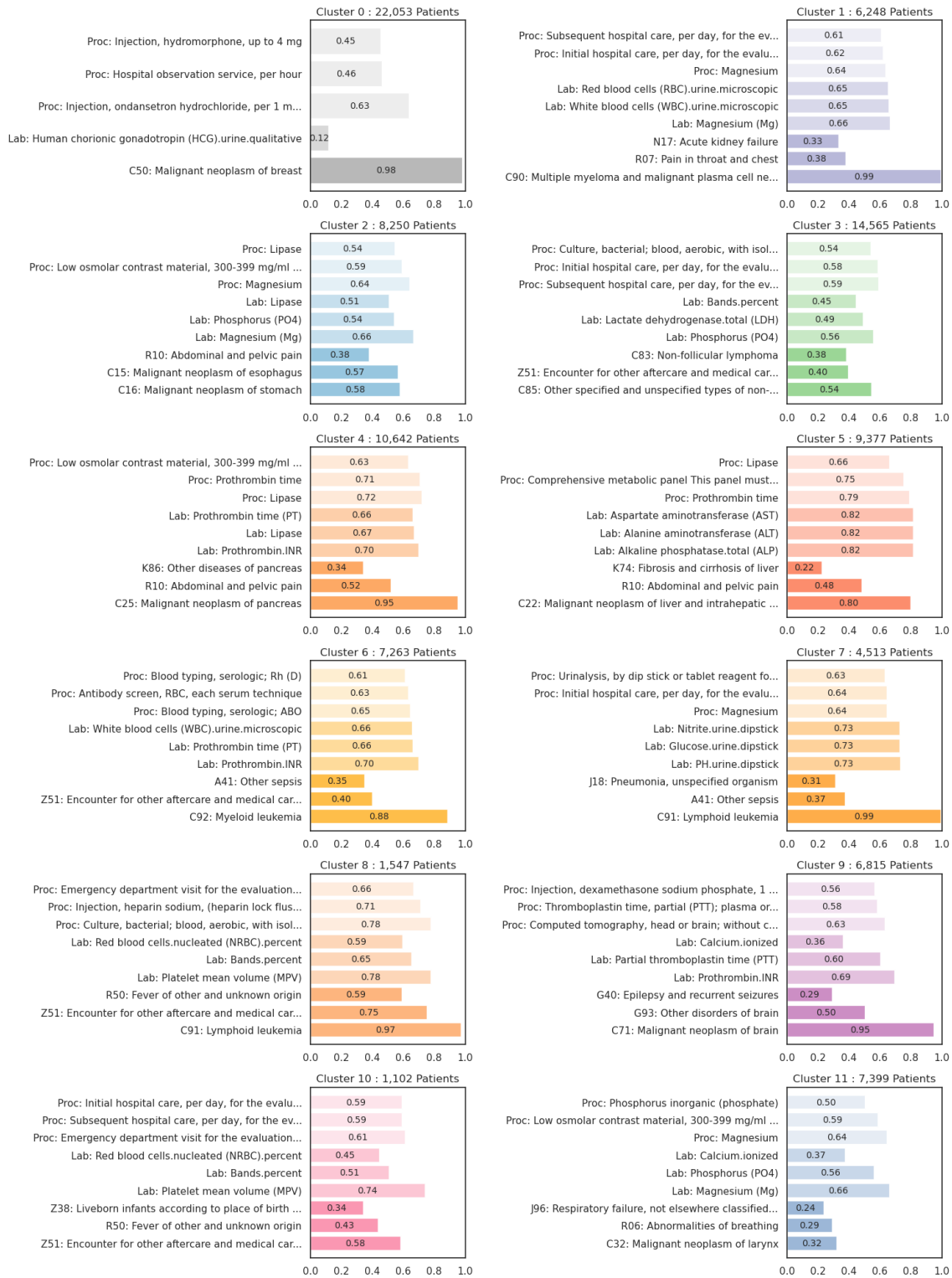


Figure 13: The three most common procedures, labs and diagnoses for the clusters 0-11 identified by HDBSCAN. Each concept listed occurs within this cluster at least 5% more often than in the overall cohort.

ExBEHRT

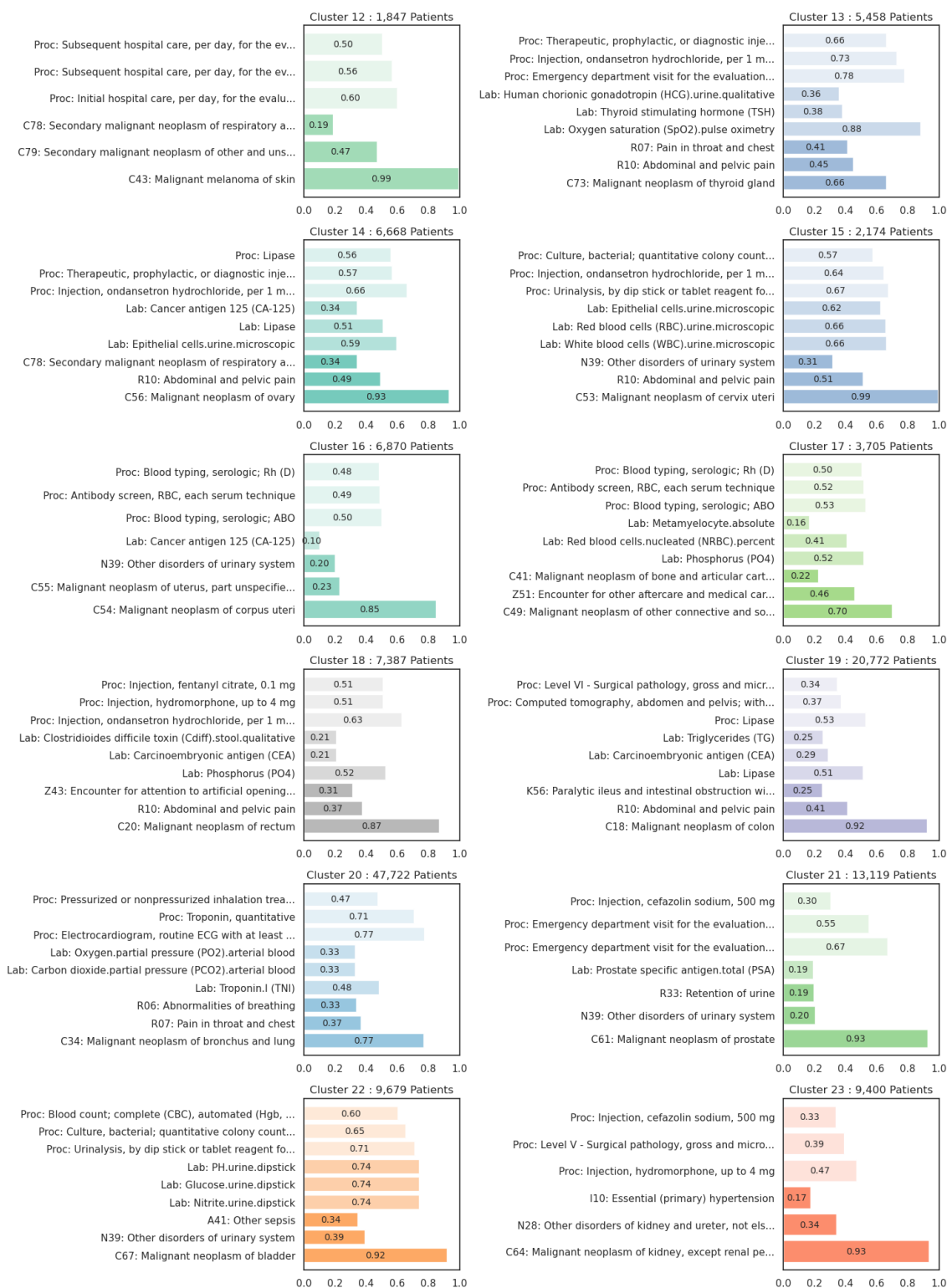


Figure 14: The three most common procedures, labs and diagnoses for the clusters 12-23 identified by HDBSCAN. Each concept listed occurs within this cluster at least 5% more often than in the overall cohort.

Appendix F. Interpretability

Table 15: The corresponding diagnoses, procedures and labs for each slot of the patient used with the Self-Attention visualization methodology. The patient journey is cut at the first cancer diagnosis.

Slot	Diagnosis	Procedures	Labs
1	E11	36415, 80076, 93041, 96374	Chemistry, urinalysis
2	R55	80048, 85025, 94760, 99284	Hematology, blood gas
3	J40	36415, 71020, 80053, 83880, 85025, 93005, 93041, 94760, 96360, 99284, A9270	-
4	M17	-	-
5	S13	72100, 73520, 96372, J1885	Blood gas
6	M54	72125, 94760, 99285	-
7	C34	99223	Chemistry
8	J18	93306	Hematology
9	I46	93010	Blood gas
10	R06	99232	-
11	J96	-	-
12	I49	-	-
13	J15	-	-
14	R07	-	-